Desalination and Water Treatment
www.deswater.com
doi: 10.5004/dwt.2019.23818

152 (2019) 283–298
June

Adsorption of Pb(II), Cu(II) and Ni(II) ions on functionalized carbon nanotube-C60 hybrid: adsorption process, isotherm, thermodynamic and kinetic studies

Najmeh Mehrmand[a], Mostafa Keshavarz Moravaji[a,b,*], Arsalan Parvareh[a,c]

[a]*Department of Chemical Engineering, Borujerd Branch, Islamic Azad University, Borujerd, Iran, emails: moraveji@aut.ac.ir (M.K. Moravaji), naj451.mand@gmail.com (N. Mehrmand), a.parvareh@razi.ac.ir (A. Parvareh)*
[b]*Department of Chemical Engineering, Amirkabir University of Technology (Tehran Polytechnic), Tehran, Iran*
[c]*Chemical Engineering and Petroleum Faculty, Razi University, Kermanshah, Iran*

Received 17 October 2018; Accepted 17 January 2019

ABSTRACT

In this study, the functionalized carbon nanotube-C60 hybrid was tested for the adsorption of the heavy metals. The results of this study showed that the hybrid is suitable to remove heavy metal ions such as copper, nickel and lead from aqueous solutions. The experiment was conducted at varying contact time, adsorbent dose, adsorbate concentration and pH, from 30 to 180 min, 0.04 to 0.1 g, 10–50 mg L^{-1} and 2–8, respectively. Most of the significant changes are observed at 30 min of contact time, 0.06 g of the adsorbent and 20 mg L^{-1} of the adsorbate concentration. Maximum percentage removal was obtained for Pb, Cu and Ni ions at pH of 5 with the lowest amount of the precipitate (≈94%, 90.65% and 2.4%) and at pH of 7 with the highest amount of the precipitate (≈99.96%, 99.88% and 99.50%), respectively. Four kinetic and isotherm models are used for predicting the kinetics and mechanisms of adsorption by calculating the correlation coefficient and their parameters. The results showed that the best mechanisms of adsorption model and correlation coefficient (R^2) of metals follow for Pb (D-R, 0.999 and Langmuir, 0.966), Cu (D-R, 0.965) and Ni (Freundlich, 0.961 and Temkin, 0.965). At pH 7 for each of the three metals, ΔG is negative (reaction spontaneous) and at pH 5, reaction is spontaneous for lead and copper, and non-spontaneous for nickel. At pH 5–7, ΔHs are negative, thus the reactions are exothermic. The best kinetic models and correlation coefficient (R^2) that seem to explain better the experimental data are for lead, copper and nickel are pseudo-second-order, 0.999; pseudo-second-order, 0.999 and pseudo-first-order, 0.981, respectively.

Keywords: Functionalized nanotube-C60 hybrid; Percentage removal; Kinetic models; Adsorption isotherm; Isotherm models; Heavy metal

1. Introduction

Water is one of the most essential elements of life on Earth and has solutions mineral that are important for the survival of organisms [1]. The population has grown seven times from 1800 to 2011, estimated at 7 billion. Accelerating population growth, pollution and climate change will lead to a sharp decline in water over the coming decades [2]. In 2013, about 1.1 billion people used nanotechnology to access safe drinking water and 2.4 billion people lacked access to appropriate hygiene (mostly in developing countries). By 2025, the world's population is expected to be over 9 billion which the under water pressure countries and consumption of water will increase to two thirds and 55%, respectively [3]. The main reasons for the pollution of water resources are chemical and biological contaminations, the increase of urbanization and the development of industries and agriculture.

* Corresponding author.

Water pollutants can be divided into three categories: organic, inorganic and biological pollutants. Mineral contaminants are in the category inorganic such as heavy metal, which are mostly due to industrial activities such as metalworking, chemical production, metallurgical industry, mining operations, soils around military bases and handicrafts that can enter water resources [4,5].

The most common pollutants of heavy metals are Cd, Cr, Cu, Hg, Pb, Zn, Ni, Cr, etc. They are toxic due to cumulative effects and their interference with the biochemical function of cells for plants, animals and humans. Heavy metals are one of the most dangerous harmful pollutants due to the lack of biodegradation, long biologic half-life and accumulation capacity in aquatic ecosystems [6,7]. There are many methods to remove metal ions from wastewater before entering water sources. These methods are used to remove or reduce metal ions including oxidation, precipitation, membrane filtration, ion exchange, adsorption, evaporation and condensation, reverse osmosis and electrolysis [8–13].

Most of these methods are incompatible with the environment, need high power and expensive [14]. The nanotubes, C60s and activated carbon are carbon-based nanoparticles, which are often used to adsorb a wide variety of water pollutants. The findings indicate that the nanotubes, C60s and activated carbon [15] have a large potential for removal of many pollutants [16–22]. C60s are generally insoluble; hence, by adding a suitable group the solubility can be increased [23]. Functionalized C60s are divided into two categories:

- Exohedral C60s with molecules out of cage such as (C60H8) [24].
- Endohedral C60s with molecules trapped inside the cage. The first lanthanum C60 complexes were built in 1985 and named the lanthanide endoc60s, La @ C60 [25].

Although raw carbon nanotubes cannot be intrinsically solved in aqueous solutions due to the strong adsorption of the Van der Waals forces along the tubes, many new materials have been made to increase their solubility and also to use their properties by adding agent groups to side walls for modifying the surface of carbon nanotubes [26]. The carbon nanotube-C60 hybrid was first discovered by Luzzi [27], which revealed that multiple C60s as a by-product in the synthesis of single-walled carbon nanotubes (SWCNs) were trapped inside the open-ended nanotubes. In this study, the functionalized C60 and nanotube were used, a hybrid produced that is used for adsorbing heavy metals of aqueous solutions.

2. Materials and synthesis method

Materials for the synthesis of nanotube-C60 hybrid are manufactured by the Emfutur Company from Spain. The synthesis of the hybrid is based on the studies of Bourlinos et al. [28]. In this research, pure fullerene after oxidation was used instead of fullerol sodium salt for hybrid synthesis.

2.1. C60 oxidation

3 g of pure C60 was added to 750 mL of concentrated nitric acid (67%). The mixture was suspended by sonication for 10 min in order to disperse more C60. Then, the temperature of the mixture was slowly raised up to 115°C and the mixture was refluxed for 6 h. After cooling materials at ambient temperature, the mixture was washed with the de-ionized water several times, until solution pH reaches 7, and in order to completely dry, the solids were heated at 80°C. The final products are dark brown solids (oxidized C60), which are soluble in water.

2.2. Synthesis of nanotube-C60 hybrid

3 g of oxidized C60 were suspended in 300 mL of deionized water by sonication for 10 min in order to disperse more. 9 g of carboxylic nanotube were suspended in the above mixture by sonication for 10 min (the amount of oxidized C60 to carboxylic nanotube is 1:3 weights). The mixture was refluxed for 6 h and then heated at 80°C for 8 h for evaporating the water. The residue solids were heated at 200°C for 24 h and then were washed with the de-ionized water several times until the solution pH reaches 7. This action is done to remove the soluble particles in the previous steps. Finally, the solids were dried at 80°C and used as hybrids in the sorption experiments.

3. Method experimentals and analyses

3.1. Method experimentals

Lead, copper and nickel nitrate are selected for the hybrid adsorption performance. For the better investigation of conditions of the polluted waters, three metals with equal concentration are used as multi-metals adsorption.

The effects of contact time, adsorbent dose, pH, initial concentration, thermodynamic, isotherm and kinetic adsorption models were examined in this study. Minitab has been used to draw shapes.

Experimental conditions: the adsorption process was investigated at 25°C, 50 mL of the metal solutions, 0.04–0.1 g of the adsorbent with 0.02 intervals, contact time of 30–180 min with 30 min intervals., pH of 2–8, initial concentration of heavy metals 10–50 mg L^{-1} and agitation speed at 100 rpm. The adsorption process is carried out in batch mode. The optimal adsorbent dose and the contact time were determined. Then, the effects of pH and initial concentration of heavy metals are investigated to obtain the optimal pH and initial concentration. Sodium hydroxide (NaOH 1 mol L^{-1}) and nitric acid 65% (HNO_3 1 mol L^{-1}) are used to adjust the pH. With regard to the solubility of the nitrates, which are soluble, when metal nitrates are mixed with NaOH, precipitates of metal hydroxides are formed along with sodium nitrate. The metal hydroxides are usually insoluble that depends on the pH of the final solution and temperature. If a drop or more of NaOH is added to a very acidic solution, nothing would happen since the solution would still be acidic. However, if the solution becomes alkaline, the precipitates of the metal hydroxides are formed (Table 1).

Table 2 shows that the solubility of the nickel, lead and copper nitrate is reduced, respectively. For this reason, in the metal solutions without adsorbent, the metal hydroxides precipitate in the environments toward alkaline. To analyze the results, it is necessary to pay more attention to the

Table 1
Equations for the reaction of heavy metals in acidic and alkaline environments

Heavy metal	pH	Equations reaction
Nickel(II) nitrate	Base	$Ni(NO_3)_{2(aq)} + 2NaOH_{(aq)} = 2NaNO_{3(aq)} + Ni(OH)_{2(s)}$
	Acid	$Ni(NO_3)_2 + HNO_3 = Ni(NO_3)_2 + NO_2 + H_2O$
Copper(II) nitrate	Base	$Cu(NO_3)_{2(aq)} + 2NaOH_{(aq)} = Cu(OH)_{2(s)} + 2NaNO_{3(aq)}$
	Acid	$Cu(NO_3)_2 + HNO_3 = Cu(NO_3)_2 + NO_2 + H_2O$
Lead(II) nitrate	Base	$Pb(NO_3)_{2(aq)} + 2NaOH_{(aq)} = Pb(OH)_{2(s)} + 2NaNO_{3(aq)}$
	Acid	$2H_2O + Pb(NO_3)_2 \rightarrow 2HNO_3 + Pb(OH)_{2(s)}$

Table 2
Solubility of metals compounds solutions in water

Solubility in water (g/100 mL water) [29]			
Substance	Formula	20°C	30°C
Nickel(II) nitrate	$Ni(NO_3)_2$	94.2	105
Lead(II) nitrate	$Pb(NO_3)_2$	54.3	63.4
Copper(II) nitrate	$Cu(NO_3)_2$	125	156
Sodium nitrate	$NaNO_3$	87.6	94.9
Sodium hydroxide	NaOH	109	119
Copper hydroxide	$Cu(OH)_2$	1.722×10^{-6}	–
Lead hydroxide	$Pb(OH)_2$	1.615×10^{-4}	–
Nickel hydroxide	$Ni(OH)_2$	0.013	–

chemical reaction of these metal solutions in the acidic and alkaline environment and their solubility in the temperature range of 20°C–30°C.

3.2. Analyses

3.2.1. SEM analyses

The morphologies of nanomaterials are measured with FE-SEM (Mira3 LMU, Tescan). In Figs. 1(a) and (b) show that the measured outer diameters (ODs) before and after adsorption for the hybrid are 33.23–43.25 and 34.97–45.20 nm, respectively. The OD for the carboxyl nanotube and C60 is 20–30 nm and 1 nm, respectively. The minimum diameter before and after sorption of the hybrid is greater than the maximum total diameter of carboxylic nanotube and C60, which indicates before sorption, the oxidized C60 agents

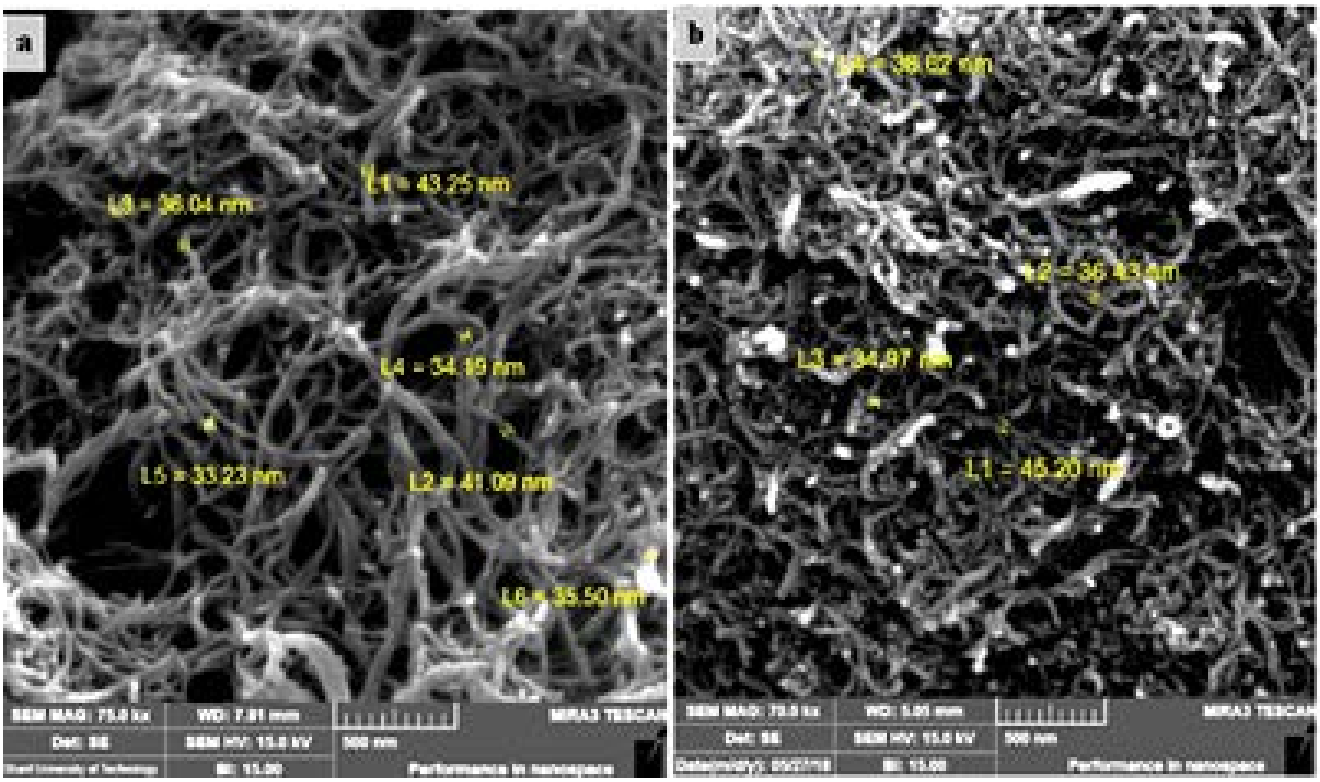

Fig. 1. FE-SEM morphology of hybrid: (a) before adsorption, OD = 33.23–43.25 nm and (b) after adsorption, OD = 34.97–45.20 nm.

are placed on the surface of carboxylic nanotubes. Also, after sorption, oxidized metals are located on the surface of hybrids.

3.2.2. XRD analysis

The XRD diagrams of CNT–COOH, C60 $(OH)_n$, hybrid, and comparison between CNT–COOH and hybrid are shown in Figs. 2(a)–(d). These diagrams indicate that there are C60$(OH)_n$ compounds in the hybrid. According to Table 3, the highest peaks in the CNTs–COOH and hybrids are shown in the 2θ = 25.85, 6.83, 12.41, 18.38, 14.38 and 2θ = 25.76, 20.90, 10.94, 17.87, 8.50, respectively. It is clear the nanotubes have been covered with oxidized C60 which are clearly observed in Fig. 2(d).

3.2.3. FTIR analysis

The FTIR spectra of the hybrid were recorded in the range of 4,000–400 cm^{-1}. The existence of the types of functional groups is confirmed by two diagrams of hybrid before and after adsorption that has been shown in Fig. 3.

The peak located at 1,735.916 cm^{-1} with change percentage transmittance of 2.064 to 5.078 is due to stretching

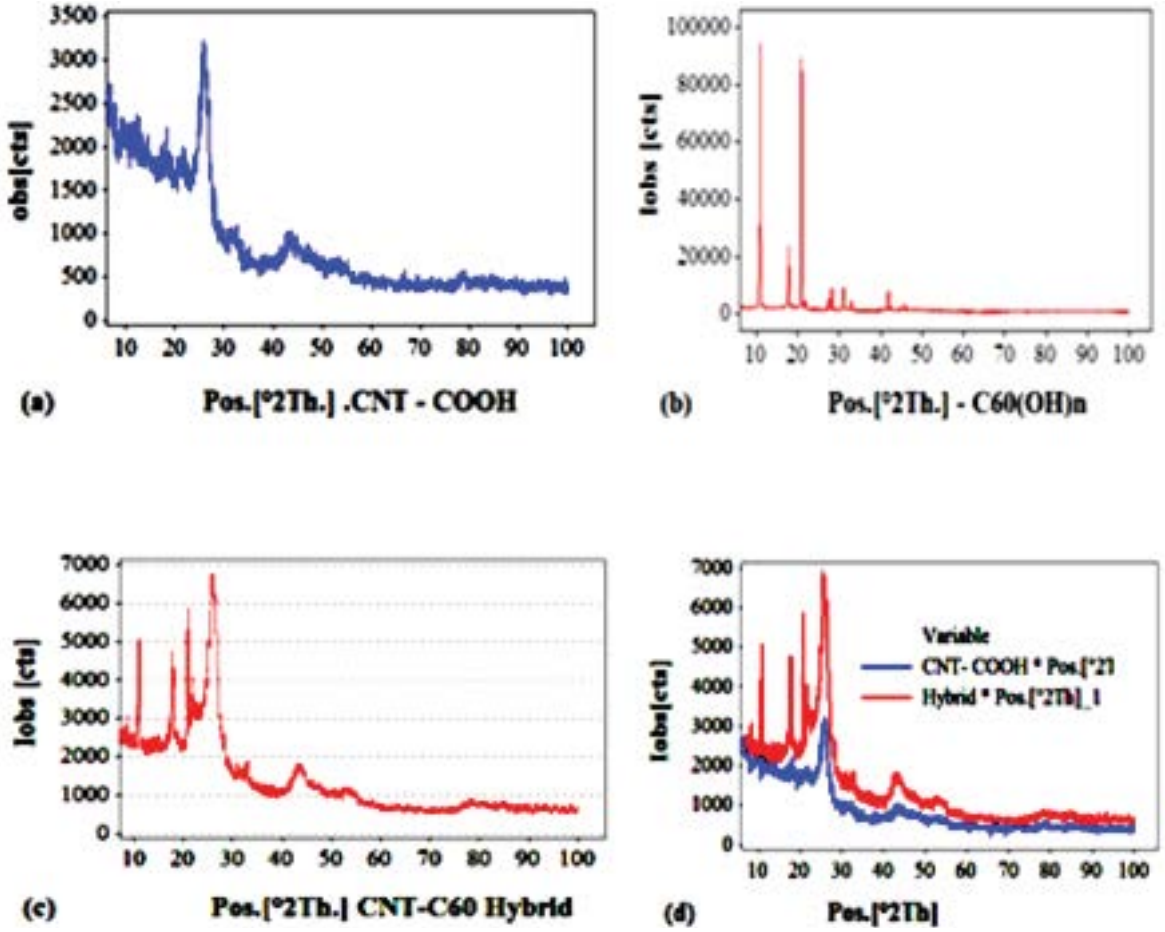

Fig. 2. XRD patterns of (a) CNT–COOH, (b) C60$(OH)_n$, (c) hybrid and (d) CNT–COOH and hybrid.

Table 3
Highest values of XRD peaks for different samples

Samples	CNT-C60 hybrid		C60 oxide		CNT–COOH	
	2θ°	lob (cts)	2θ°	lob (cts)	2θ°	lob (cts)
Decrease peak	25.76	6,765.41	10.94	94,368.85	25.85	3,230.00
	20.90	5,862.37	31.01	93,761.00	6.83	2,728.80
	10.94	5,078.08	20.90	89,239.60	12.41	2,327.91
	17.87	4,728.12	17.81	22,352.00	18.38	2,163.90
	8.50	3,084.83	28.21	8,863.57	14.38	2,140.29

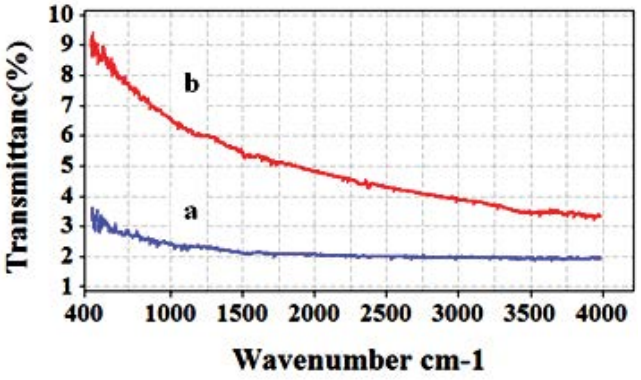

Fig. 3. FTIR spectra of hybrid (a) before adsorption and (b) after adsorption of metal ions.

of the carbonyl group. The peaks at 1,624.046; 1,450.45 and 1,201.64–1,274.93 cm^{-1} are related to the stretching vibration of the carboxyl(–C=O), carboxylic(–COO–) and C–O groups, respectively. The peaks at 3,439.042 and 3,234.59 cm^{-1} are related to the stretching vibration of the $C60(C(COOH)_2)_2$ and $C60\ (OH)_n$, respectively. Fig. 4(b) shows the FTIR spectrum of Pb, Cu and Ni(II)–adsorbed on the hybrid. Due to the interaction of the functional groups on the hybrid with metal ions, the percentage transmittance and IR peaks shift to higher values. Shifting to lower and higher frequencies is an indication of motion of weaker and stronger bonds, respectively [29].

The bands in the region 400–800 $cm^{-1}$are assigned to stretching vibrations of the meta-oxygen. The percentage transmittance changes from 3.288 to 8.883 at band 499.409 cm^{-1} and 2.641 to 7.268 at 800.45 cm^{-1} that corresponds to the asymmetric stretching vibration of metal oxide linkage.

3.2.4. BET analysis

The analysis data of the BET surface area of hybrid suggest that the surface area, size and total volume of the pore can change before and after adsorption. The parameters are shown in Table 4. By looking at Table 4, one can see that the surface area of hybrid is large. The BET surface area ($m^2\ g^{-1}$), adsorption average width (nm) and Single point adsorption total pore volume of pores ($cm^3\ g^{-1}$) for the diameters less than 85.3896 and 102.2139 nm of the hybrid before

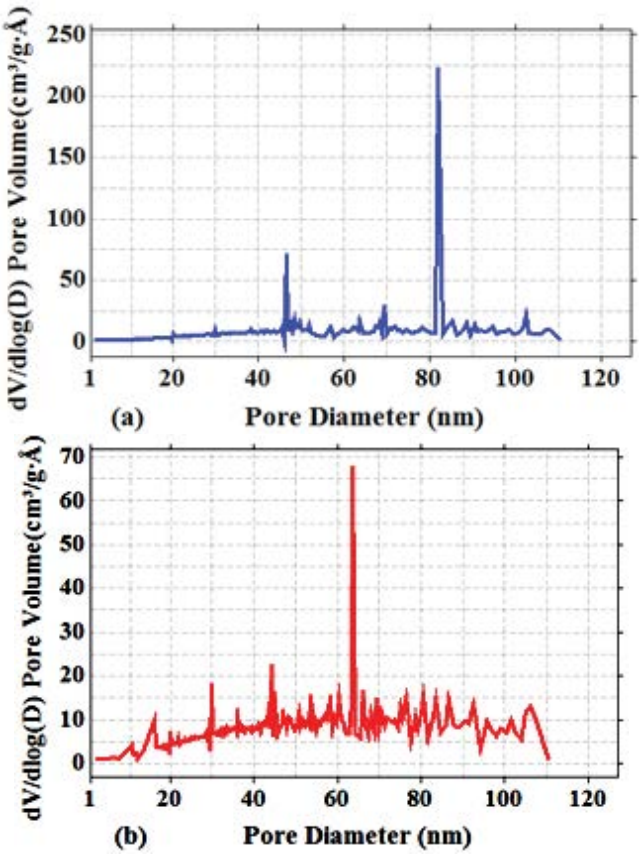

Fig. 4. Pore size distribution plots of the hybrid, (a) before adsorption and (b) after adsorption.

adsorption are 1,625.93, 15.9, (6.46, 7.40), and after adsorption reaches 1,592.67,17.20, (6.86, 7.82), respectively. Figs. 4(a) and (b) show that the main peak is centered at pore diameter equal to 82.10535 and 63.64649 nm before and after of adsorption, respectively

4.1. Effect of contact time

Time is an important parameter in the processes and by selecting suitable contact time, the processes were done at high speed and low cost [31].

Table 4
Results of BET surface area analysis of hybrid before and after adsorption

Parameter of pores	Type of adsorption	Before adsorption	After adsorption
Surface area ($m^2\ g^{-1}$)	BET	1,625.93	1,592.67
	Langmuir	2,190.62	2,149.03
	BJH	1,860.75	1,342.91
Single point adsorption total pore volume (cm^3/g)	Diameter < 85.3896 nm	6.46	6.86
	Diameter < 102.2139 nm	7.40	7.82
Adsorption average width (nm)	Adsorption BET	15.9	17.2
	Adsorption BJH	15.8	22.1

BET, Brunauer–Emmett–Teller; BJH, Barrett–Joyner–Halenda.

The removal percentage for each of the three metals depends on the contact time, which is shown in Figs. 5(a)–(d). At pH 2, the sorption of each of the three metals is negligible. In Fig. 5(a), at pH 5, it is observed that the optimal contact time is 30 min and at 30 min, the percentage removal of lead and copper are more than 90% and nickel is less than 20%. The sorption of lead and copper is very quick and lower than 1 h is sufficient to achieve the equilibration while the sorption of nickel is very slow. At pH 5, in the absence of the adsorbent, only the lead ions are precipitated. At pH 8, in the absence of the adsorbent, each of the three metals precipitates and at 30 min, the removal percentage of the three metals is more than 99%.

4.2. Effect of adsorbent dose

The adsorption experiments were carried out by using various adsorbent dose 0.04–0.1 g with 0.02 intervals. By increasing the adsorbent dose from 0.04 to 0.06 g, the removal percentage of metals is rapidly increased because the number of adsorption sites is proportional to the number of metal ions. With further increase of the amount of adsorbent from 0.06 to 0.1 g, despite the abundant number of unsaturated adsorption sites due to the limited number metal ions, the removal percentage is reduced and thus the unsaturated sites remain free. The maximum removal is shown at 0.06 g of hybrid that is selected as an optimum dose. At the optimum dose, the removal percentage of Pb, Cu and Ni are obtained to be 94, 90.65 (Fig. 6(a)) and 0.85 (Fig. 6(b)), respectively.

4.3. Effect of pH

The amount of pH is an important factor in the adsorption of metal ions on the adsorbent. At a lower pH (pH ≤ 4), metals have a negative charge while the surface of the adsorbent is charged positively. Amount of acidity solution is used to neutralization of surface charge; thus the adsorption of cations should decrease. The metal adsorption increases as pH increases. When pH of the solution is increased, the surface becomes more negatively charged; the interactions between species are electrostatic that favors the adsorption of cations.

The obtained results indicate that the adsorption of lead, copper and nickel ions is increased with the increase of pH from 2 to 8, but a sharper increase of pH is observed for lead and copper at 4–5 and for nickel 5–7. The low adsorption of metals is placed in an acidic region that is created a competition between H^+ and M^{+2} ions on the adsorption sites and the charge on the surface becomes more negative, Figs. 7(a)–(d). In the absence of adsorbent, the lead, copper and nickel ions begin to precipitate at pH 4, 5 and 6, respectively, while the concentration of metals in the liquid phase is reduced in the presence of adsorbent (w = 0.06 g). Therefore, the optimal pH is at the region that the distance between two graphs the adsorption of the metal (red) and the formation of

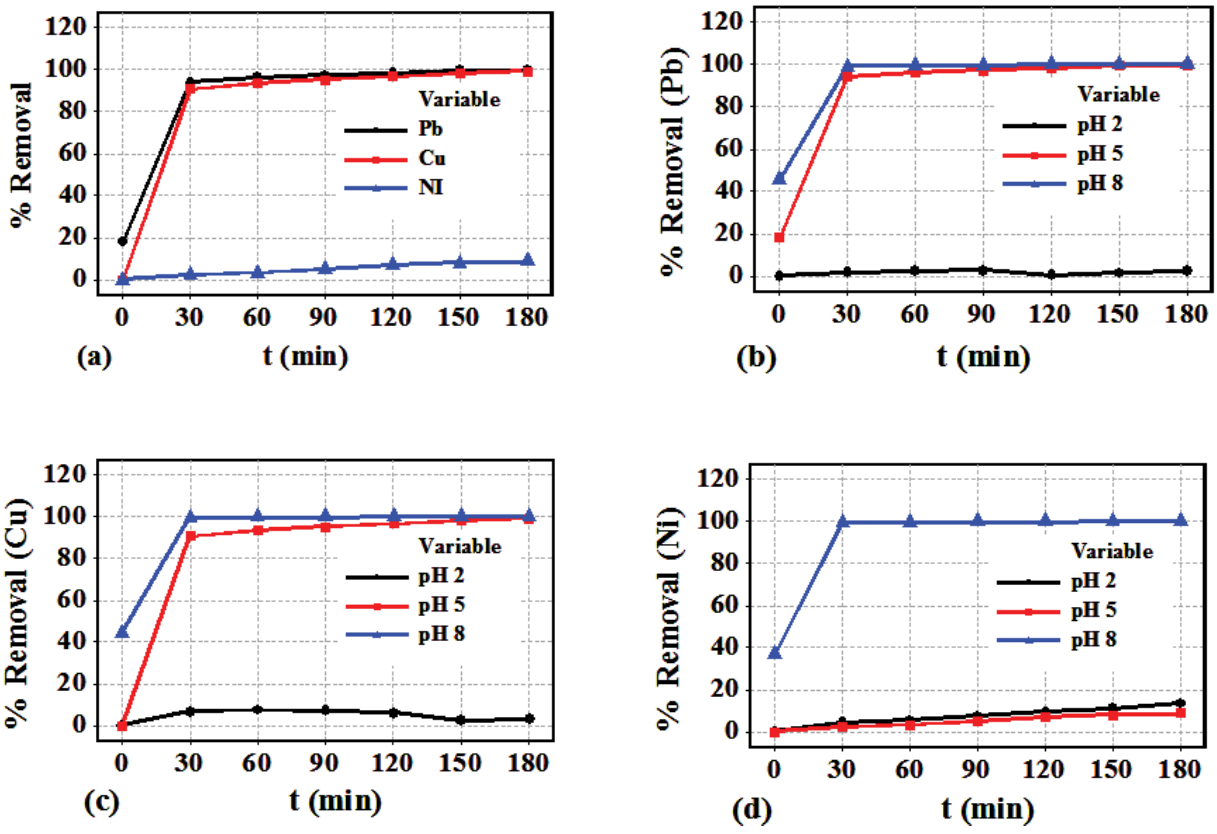

Fig. 5. Changes in percentage removal of heavy metals with time, (a) each three metal at pH 5, (b) Pb, (c) Cu, and (d) Ni, at pH 2, 5, 8 (T = 25°C, C_i = 20 mg L^{-1}, w = 0.06 g).

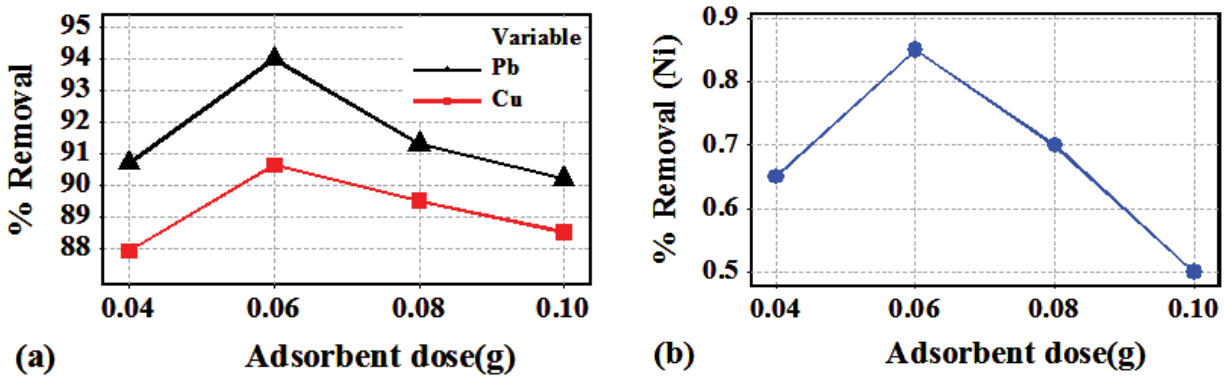

Fig. 6. Changes in the percentage removal with adsorbent dose for (a) lead and copper and (b) nickel (T = 25°C, C_i = 20 mg L^{-1}, t = 30 min, pH = 5).

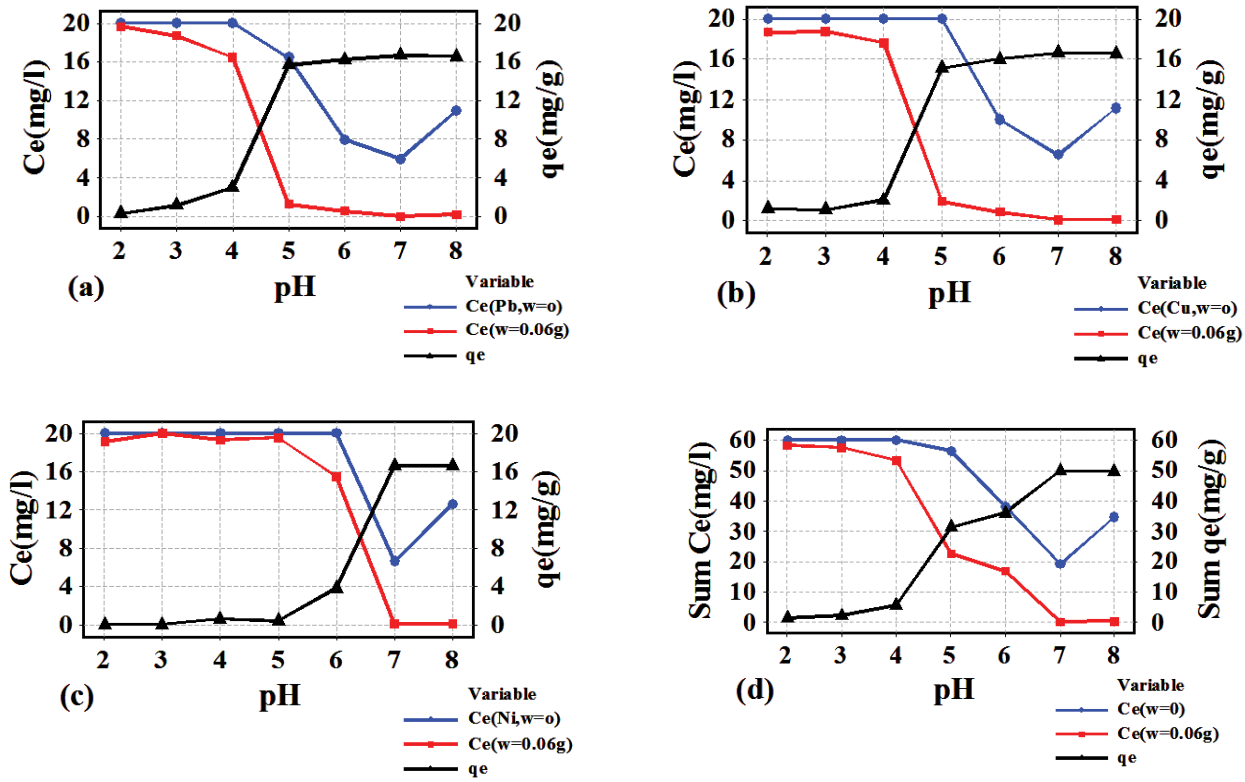

Fig. 7. Effect of pH on the adsorption capacity and the concentration of (a) lead, (b) copper, (c) nickel metals and (d) sum of three metals (T = 25°C, C_i = 20 mg L^{-1}, t = 30 min, w = 0.06 g).

the precipitation (blue) is maximum, also in this region, the adsorption capacity is often high (Fig. 7).

For better interpretation of adsorption, the changes in total concentration of the metals is considered. When the pH rises from 2 to 8, the concentration of metals in the liquid phase changes from 58.3 to 0.345 mg L^{-1}. Therefore, the optimal pH is 5, which the lowest precipitate and the high adsorption of metal are obtained (Fig. 7(d)). In the acidic environment, the removal percentage of metals is greatly reduced, as the repulsion is increased on the hybrid.

The removal percentage for lead, copper and nickel, at pH 5 is 94%, 90.65% and 2.4%, with the lowest sediment content and at pH = 7 is 99.96%, 99.88% and 99.45% with the highest sediment content, respectively. The graphs show that the suitable pH for nickel is between 7 and 8, for lead and copper is between 5 and 6 (Fig. 8).

4.4. Effect of the initial concentration

By increasing the initial concentration from 10 to 50 mg L^{-1}, the removal percentage of lead, copper and nickel from 95.8, 90, 36.9 reaches 45.5, 43, 8.72, respectively (Fig. 9). By increasing the initial concentration, the removal percentage of metals is decreased and thus the removal percentage

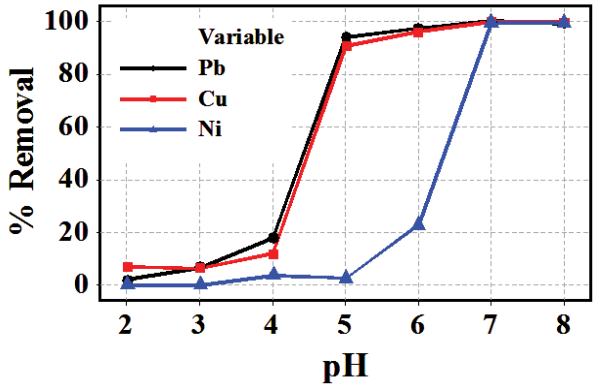

Fig. 8. Effect of pH on the removal percentage of metals (T = 25°C, $C_{i\ \mathrm{Metal}}$ = 20 mg L^{-1}, t = 30 min, w = 0.06 g).

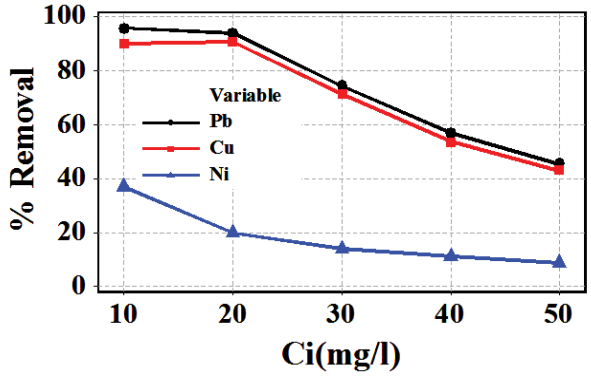

Fig. 9. Changes in percentage removal of metals with the initial concentration (T = 25°C, pH = 5, t = 30 min, w = 0.06 g).

depends on the initial concentration of metals. At low initial concentrations, there are fewer metal ions that are ready to adsorb on a certain number of unsaturated hybrid sites. At higher concentrations, there are more metal ions that remained free in the solution because all adsorption sites are saturated. It is observed that the optimal amount of initial concentrations is 20 mg L^{-1}, which after this concentration, the removal percentage is decreased.

By changing the initial concentration of metal solutions at pH = 5, it is observed that the adsorption capacity for lead and copper is fast to equilibrium whereas, for nickel, it happens at a higher pH. The maximum adsorption capacity for lead, copper and nickel at pH = 5 is 19, 17.9 and 3.9 mg g^{-1}, respectively (Fig. 10).

4.5. Adsorption isotherm models for experimental data

Sorption of sorbates on any sorbent can occur either by physical bonding, ion exchange, complexation, chelation or through a combination of these interactions. The interaction between sorbent and sorbate molecules not only are physical bonding but also the another mechanism of adsorption can be [32]. Physical adsorption is easily demonstrated by using distilled water. If the solubility adsorbent increases in the distilled water, it indicates that there are functional groups such as hydroxyl, carbonyl and carboxyl, etc. in the structure of the adsorbent.

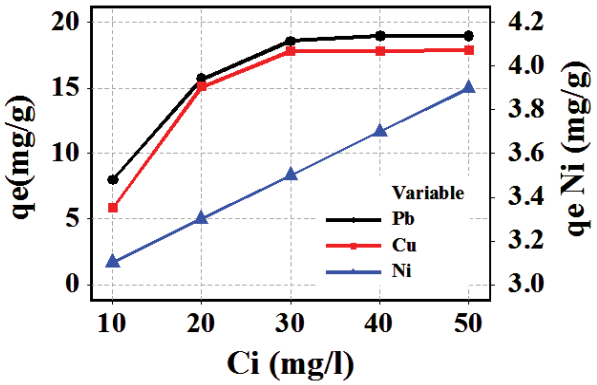

Fig. 10. Changes in adsorption capacity of metals with the initial concentration (T = 25°C, pH = 5, t = 30 min, w = 0.06 g).

Investigations and studies on the adsorption of isotherm have led to the discovery kind of models. In this study, four linear Langmuir, Freundlich, Dubinin–Radushkevich and Temkin models have been used to describe the adsorption data.

Non-linear Langmuir isotherm model shows that the nickel adsorption capacity increases with increasing metals concentration. It means that this pH is not suitable for adsorption of nickel. For lead and copper, by increasing the initial concentration, the adsorption capacity is fixed (Fig. 11).

These four adsorption isotherm models have been described as follows:

4.5.1. Langmuir

In the Langmuir adsorption model, it is assumed that: (1) a layer of adsorbent material, (2) uniform adsorbent surface (3) without any interaction between absorbed ions [33,34].

Two other parameters, the separation factor (RL) and surface coverage (θ) are for the better description of the Langmuir model that used to adsorption isotherm. Eqs. (1)–(3) indicate the Langmuir model, the separation factor and surface coverage equations.

$$\frac{1}{q_e} = \left(\frac{1}{K_L q_m}\right)\frac{1}{C_e} + \frac{1}{q_m} \tag{1}$$

$$R_L = \frac{1}{1 + K_L C_i} \tag{2}$$

$$\theta = \frac{K_L C_i}{\left(1 + K_L C_i\right)} \tag{3}$$

where q_e is the adsorption capacity at equilibrium (mg g^{-1}), q_m is the maximum adsorption capacity (mg g^{-1}), C_e is the equilibrium concentration and C_i is the initial concentration of adsorbate (mg L^{-1}) and K_L is the Langmuir isotherm constant (L mg^{-1}).

4.5.1.1. In the adsorption of the Langmuir model

The amount of K_L for lead, copper and nickel is 1.57, 0.47 and 0.37, respectively, that indicates the adsorption of

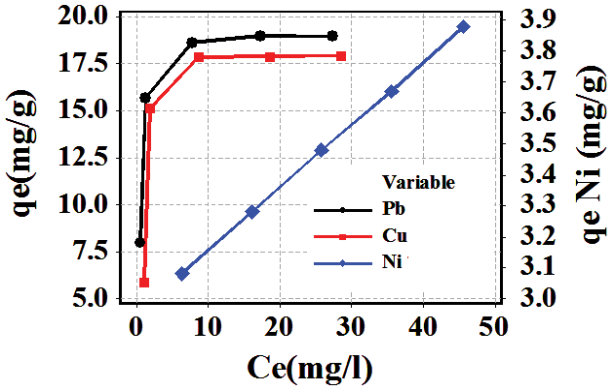

Fig. 11. Non-linear Langmuir isotherm model for the metals Pb, Cu and Ni (pH = 5, T = 25°C, w = 0.06 g, t = 30 min, C_i = 10–50 mg L^{-1}).

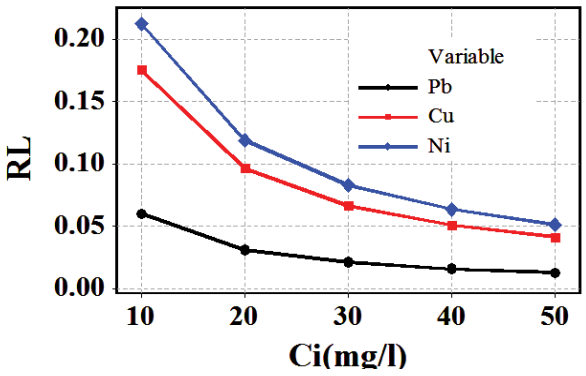

Fig. 12. Changes in separation factor (RL) with initial concentration (pH = 5, T = 25°C, w = 0.06 g, t = 30 min).

lead is stronger than copper and nickel. The larger K_L value represents a stronger adsorption. The calculated maximum adsorption capacity (q_m) of lead (20.6), copper (25.36) and for nickel (2.87) is more than the experimental data. The calculated maximum adsorption capacity (q_m) may be smaller or larger than the adsorption capacity of experimental data due to the abundance of adsorbent sites, the number of ions that can affect the surface adsorbent and the binding intensity of ions to the surface.

4.5.1.2. Separation factor (RL)

Changes in amount of separation factor (RL) are for lead (0.013–0.06), copper (0.04–0.177) and nickel (0.051–0.213) when the initial concentration changed from 10 to 50 mg L^{-1}. The separation factor value (RL) for three metals is between zero and one; therefore, the adsorption process is favorable. With regard to the following description, the adsorption is not very strong, but its amount is considerable (Fig. 12).

- RL = 0 irreversible adsorption occurs if K is very large, which means that adsorption is too strong.
- 0 < RL < 1: This is the standard case when adsorption occurs normally under experimental conditions. Not so strong, but noticeably occurs. The shape of the adsorption is isotherm that is a favorable adsorption.
- RL = 1: This adsorption is linear adsorption (only if K = 0).
- RL > 1: if K is negative and $-1 < C_i{}^*K < 0$ but this is not possible.

If the denominator of Eq. (2) is negative, then, RL is negative, and instead of adsorption, desorption occurs and the adsorption is unfavorable [35,36].

4.5.1.3. Surface coverage

Θ is defined as the fraction of sites occupied by solute molecule. The range of surface coverage is from zero to one. The range surface coverage of the hybrid is for lead (0.63–0.65), copper (0.185–0.191) and nickel (0.148–0.152). More than 60% of the surface coverage is related to lead metal that shows that this metal has high adsorption. By increasing the initial concentration of metal solutions (10–50 mg L^{-1}), the overall surface coverage rises from 0.96 to 0.992 (Fig. 13).

4.5.2. Freundlich

In the Freundlich model, it is assumed that the adsorption process occurs at the heterogeneous surface [37] – Eq. (4)

$$\ln q_e = \ln K_F + \frac{1}{n}\ln C_e \tag{4}$$

where K_F (L mg^{-1}), $1/n$, q_e (mg g^{-1}) and C_e (mg L^{-1}) are the measured adsorption capacity, adsorption intensity, adsorption capacity and concentration at equilibrium, respectively.

In the adsorption of Freundlich model, the K_F (adsorption capacity) for lead, copper and nickel is 11.67, 9.915 and 2.578 L g^{-1}, respectively, which indicates the separation of lead metal from the liquid phase is easier than the other two metals. $1/n$ is a heterogeneous parameter; at $1/n$ smaller, the heterogeneity is greater; therefore, the closer the value to zero (n larger), the higher the homogeneity would be. According to the amount of $1/n$ (adsorption intensity), the heterogeneity increases in copper (0.211), lead (0.180) and nickel (0.093), respectively. If the value of $1/n$ is less than one, it indicates normal adsorption and also, the closer $1/n$ to one, the closer to the linear isotherm (more homogeneity). If n is between one and ten, this represents an optimal adsorption process. The n value for lead, copper and nickel are 5.546, 4.739 and 10.811, respectively. Then, the adsorption of lead and copper are desirable and the adsorption of nickel is a little undesirable because the adsorption of nickel goes toward heterogeneity.

4.5.3. Dubinin–Radushkevich

The Dubinin–Radushkevich (D-R) model is used for both homogeneous and heterogeneous surface and calculation of adsorption energy [38–40].

$$\ln q_e = \ln q_m - \beta\varepsilon^2 \tag{5}$$

$$\varepsilon = RT\ln\left(1+\frac{1}{C_e}\right) \tag{6}$$

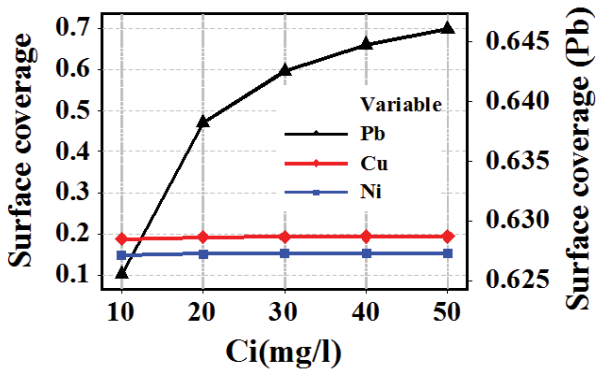

Fig. 13. Changes in surface coverage (θ) with the initial concentration (pH = 5, T = 25°C, w = 0.06 g, t = 30 min).

$$E_a = \frac{1}{\sqrt{2\beta}} \tag{7}$$

where q_e (mg g^{-1}), q_m (mg g^{-1}) and β (mol^2 kJ^{-2}) are constants which are related to adsorption capacity at equilibrium, the theory of adsorption capacity and mean free energy of adsorption, respectively. ε is a Dubinin–Radushkevich isotherm constant. C_e (mg L^{-1}), R (8.314 J mol^{-1} K^{-1}), T(K) and E_a (kJ mol^{-1}) are equilibrium concentration, the gas constant, absolute temperature and the mean energy of sorption, respectively.

In the adsorption of Dubinin–Radushkevich model, the amounts of the mean free energy (β) for lead, copper and nickel are 0.094, 0.291 and 1.162 (mol kJ^{-1})$^{-2}$. The average adsorption energy (E_a) for lead, copper and nickel is 2.31, 1.311 and 0.609 kJ mol^{-1}, respectively, which indicates that the adsorption is physical. According to the previous studies for E_a = 1–8 and E_a = 8–16 kJ mol^{-1}, is physical and chemical adsorption, respectively [41].

4.5.4. Temkin

In Temkin model, it is assumed that increasing the adsorbent coverage layer on the adsorbent surface will increase the adsorption heat of all molecules in that layer [38], (Eq. (8)).

$$q_e = \frac{RT}{b_T}\ln k_T + \frac{RT}{b_T}\ln C_e \tag{8}$$

where the parameters are: K_T, Temkin isotherm equilibrium binding constant (L g^{-1}), b_T, Temkin isotherm constant (mol J^{-1}), R, universal gas constant (8.314 J mol^{-1} K^{-1}), T, temperature at 298 K and $B\left(\frac{RT}{B_T}\right)$, constant related to the heat of sorption (J mol^{-1}).

Table 5 shows the parameters of adsorption isotherm models for the lead, copper and nickel metals.

In the adsorption of Temkin model, the amount of b_T (adsorption heat) is reduced for nickel, lead and copper, respectively. The amounts of b_T for adsorption lead, copper and nickel ions are (1.045, 0.940 and 7.550 kJ mol^{-1}), respectively. These values indicate that the adsorption of copper ions is easier than lead and nickel ions. The adsorption process is exothermic because the amount of the adsorption heat is positive. The low amount of b_T reflects the ion exchange mechanism because the typical range of bonding energy for the ion exchange mechanism is 1–8 kJ mol^{-1}. The low values of b_T in this study indicate a weak interaction between adsorbate and adsorbent. Then, the mechanism is an ion exchange for the present study.

It is observed that the best models and correlation coefficients are for lead, D-R, 0.999 and Langmuir, 0.966; for copper, D-R, 0.965 and for nickel, Freundlich, 0.961 and Temkin, 0.965 that these models are more compatible with experimental data (Figs. 14(a)–(c)).

In Table 6, the monolayer adsorption capacities for various adsorbents of the previous studies are compared with this hybrid.

4.6. Thermodynamic adsorption process

The negative amount of the free Gibbs energy indicates that the reaction is spontaneous. The positive amount of entropy and enthalpy indicates that the process is irreversible and endothermic, respectively. The negative amount

Table 5
Parameters of adsorption isotherm models for the lead, copper and nickel metals

(T = 25°C, C_i = 10–50 mg L^{-1}, t = 30 min, pH = 5, w = 0.06 g)								
Model	Freundlich				Langmuir			$q_{m,exp}$
	1/n	n	K_F	R^2	q_m	K_L	R^2	
Pb	0.180	5.546	11.67	0.745	20.6	1.57	0.966	18.9
Cu	0.211	4.739	9.915	0.659	25.36	0.47	0.876	17.9
Ni	0.093	10.81	2.578	0.961	2.87	0.37	0.62	3.6
Model	Temkin			Dubinin–Radushkevich				$q_{m,exp}$
	K_T	b_T	R^2	β	q_m	E_a	R^2	
Pb	193.60	1.045	0.806	0.094	19.03	2.31	0.999	18.9
Cu	53.45	0.94	0.72	0.291	18.52	1.31	0.965	17.9
Ni	2,916.4	7.55	0.954	1.162	3.56	0.61	0.768	3.6

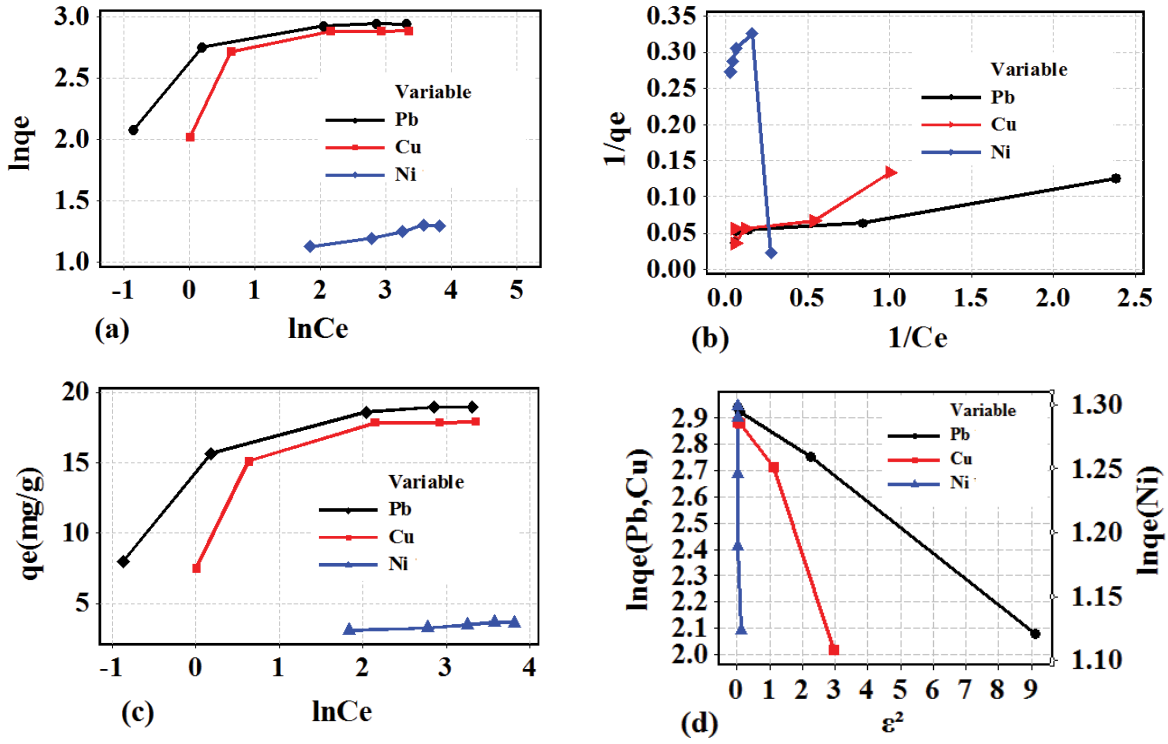

Fig. 14. Isotherm models (a) Freundlich, (b) Langmuir, (c) Temkin and (d) Dubinin–Radushkevich for lead, copper and nickel metals.

Table 6
Comparison of maximum monolayer adsorption capacities of various adsorbents

Adsorbent	Absorbed metal	q_m (mg g^{-1})	pH	Ref
Rosa canina L. leaves ash	Pb(II)	588.24	6	[42]
nFe-A	Pb(II)	833.33	6	
SDS-AZS	Pb(II)	18.38	6	[43]
Ti(IV)	Pb(II)	63.29	6	[44]
Ti(IV)	Hg(II)	21.32	6	[45]
FSAC	Pb(II)	80.65	4	[46]
MWCNTs/ThO_2	Pb(II)	More of 20	5.5	[47]
PSTM	Pb(II)	44.64	6	[48]
LELP	Ni(II)	47.61	5.5	[49]
Activated carbons	Cr(VI)	16.26	2	[15]
Nanotube-C60 hybrid	Pb(II)	18.8	8	This study
	Cu(II)	20.4		
	Ni(II)	25.2		
	Pb(II)	18.9	5	
	Cu(II)	17.9		
	Ni(II)	3.6		
	Pb(II)	1.2	2	
	Cu(II)	1.23		
	Ni(II)	0.92		

of the entropy represents a reduction in the disorder of the adsorption process due to the presence of adsorbate molecules in certain absorbent sites and the regularization of the adsorbate molecules.

The free Gibbs energy is obtained through Eqs. (9)–(11). Fig. 15 shows that Free Gibbs energy is negative at an initial concentration of 10–40 for lead and 10–30 mg L^{-1} for copper, which indicates that the adsorption process is spontaneous. When the initial concentration increases, the spontaneous reaction is reduced free Gibbs energy is positive for nickel, which increases with increasing initial concentration [50].

$$K_c = \frac{q_e}{C_e} \tag{9}$$

$$\Delta G^\circ = -RT \ln K_c \tag{10}$$

$$\Delta G^\circ = \Delta H - T\Delta S \tag{11}$$

By increasing the pH from 2 to 8, the amount of the free Gibbs energy is gradually negative, which indicates that the reaction is not spontaneous at low pHs. The changes in free Gibbs energy are positive at pH 4 to about 6.3 for nickel and at pH 2 to about 4.5 for lead and copper, which indicates that the reaction is not spontaneous, and the amount of absorption is low (Fig. 16).

For the better investigation, the adsorption process is considered in the three pHs that have the highest absorption of metal. At pH = 5, the amount of ΔG is entirely in the negative region for lead and copper. With increasing temperature from 288.15 to 313.15, and from 313.15 to 333.15 K, the amount

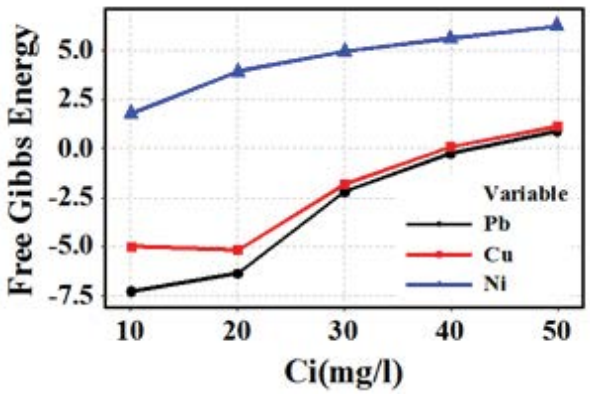

Fig. 15. Changes in free Gibbs energy with initial concentration (pH = 5, T = 25°C, w = 0.06 g, t = 30 min).

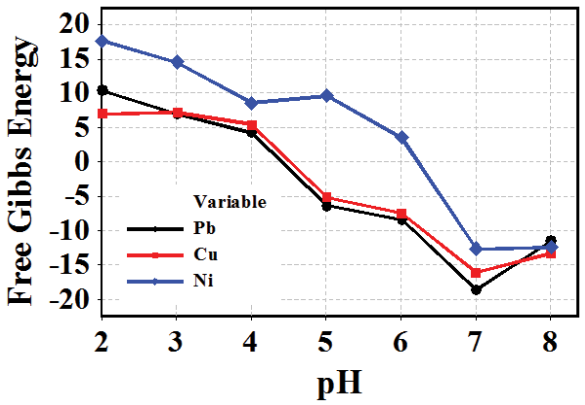

Fig. 16. Changes in free Gibbs energy with pH (T = 25°C, w = 0.06 g, t = 30 min, C_i = 20 mg L^{-1}).

of ΔG increases and decreases very little, respectively. The amount of ΔG for nickel is entirely in the positive region that shows the reaction is not spontaneous (Fig. 17(a)). At pH = 7, the amount of ΔG for metals especially nickel is entirely in the negative region; thus, the adsorption process in this pH is spontaneous (Fig. 17(b)). The amount of ΔH is negative and thus the reactions are exothermic. The negative amount of entropy indicates that the adsorption process is reversible and regular that shows the adsorbate molecules put up in certain absorption sites (Table 7).

4.7. Kinetic adsorption models

In this research, in order to study the adsorption mechanism of heavy metal ions onto the hybrid surface, we used four kinetic models, the pseudo-first-order, the pseudo-second-order, the intra-particle diffusion and the Ritchie models. The equations of the kinetic models are Eqs. (12)–(15), respectively:

4.7.1. Pseudo-first-order model

Eq. (12) introduces the pseudo-first-order model [30].

$$\ln\left(q_e - q_t\right) = \ln q_e - K_1 t \tag{12}$$

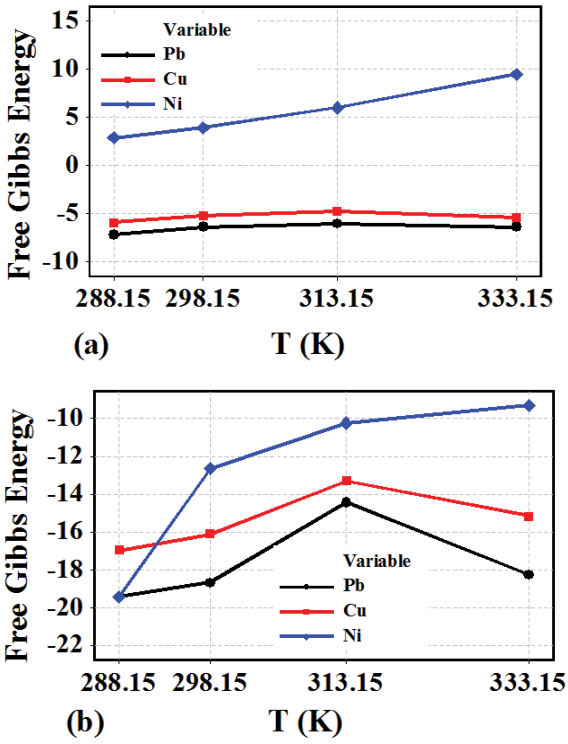

Fig. 17. Changes in free Gibbs energy with temperature at (a) pH 5 and (b) pH 7 (C_i = 20 mg L^{-1}, w = 0.06 g, t = 30 min).

where q_e is the adsorption capacity at equilibrium (mg g^{-1}), q_t is the adsorption capacity at time t and K_1 is the diffusion constant (min^{-1}; Fig. 18(a)).

4.7.2. Pseudo-second-order model

Eq. (13) introduces the pseudo-second-order model [51].

$$\frac{t}{q_t} = \frac{1}{\left(K_2 \times q_e^2\right)} + \frac{1}{q_e} \times t \tag{13}$$

where q_e is the adsorption capacity at equilibrium (mg g^{-1}), q_t is the adsorption capacity at time t, K_2 is the diffusion constant (g mg^{-1} min^{-1}) (Fig. 18(b)).

4.7.3. Intra-particle diffusion model

Eq. (14) introduces the intra-particle diffusion model [52].

$$q_t = K_{\text{id}}\sqrt{t} + C \tag{14}$$

where q_t is the adsorption capacity at time t, K_{id} is the intra-particle diffusion constant (mg g^{-1} $min^{0.5}$) and c (mg g^{-1}) is a constant that is related to the thickness of the boundary layer (Fig. 18(c)).

4.7.4. Ritchie model

Eq. (15) introduces the Ritchie model [53].

$$\frac{1}{q_t} = \frac{1}{\left(K_R q_e t\right)} + \frac{1}{q_e} \tag{15}$$

Table 7
Thermodynamic parameters for the process adsorption of heavy metals on hybrid at various pH and temperatures

						pH 5						
Ion	Pb				Cu				Ni			
T°C	15	25	40	60	15	25	40	60	15	25	40	60
Δ*G*°	–7.15	–6.37	–6.01	–6.34	–5.91	–5.18	–4.73	–5.42	2.88	3.94	6.04	9.53
Δ*H*°	–11.32				–8.26				–40.36			
Δ*S*°	–0.02				–0.01				–0.15			
						pH 6						
Δ*G*°	–9.76	–8.43	–8.01	–10.1	–8.71	–7.46	–7.42	–9.27	2.62	3.47	5.09	7.67
Δ*H*°	–5.76				–2.84				–30.14			
Δ*S*°	0.01				0.017				–0.11			
						pH 7						
Δ*G*°	–19.4	–18.7	–14.4	–18.2	–17.0	–16.1	–13.3	–15.2	–19.4	–12.7	–10.3	–9.32
Δ*H*°	–30.29				–30.17				–74.84			
Δ*S*°	–0.04				–0.05				–0.2			

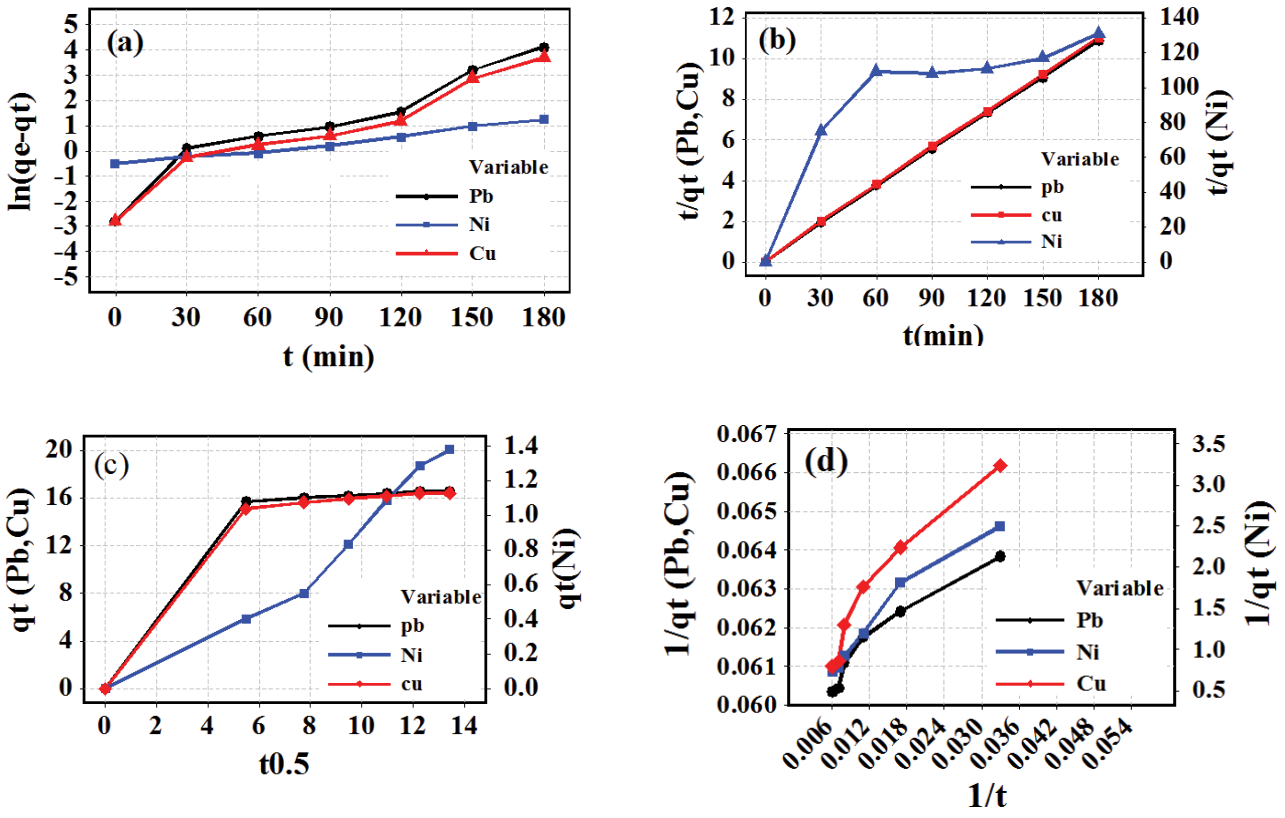

Fig. 18. Kinetics adsorption models for lead, copper and nickel (a) pseudo-first-order, (b) pseudo-second-order, (c) intra-particle diffusion and (d) Ritchie model.

where q_e is the adsorption capacity at equilibrium (mg g^{-1}), q_t is the adsorption capacity at time t, and K_R is the rate constant (min^{-1}; Fig. 18(d)).

The plots of $\ln(q_e - q_t)$, t/q_t, q_t and $1/q_t$ vs. t, t, $t^{0.5}$and $1/t$, respectively, should give a linear relationship, which the values of the adsorption parameters (K_1, q_e), (q_e, K_2), (C, K_{id}) and (q_e, K_R) can be determined from the slope and intercept of the plots in Eqs. (12)–(15), respectively (Table 8).

The $q_{e,exp}$ and the $q_{e,cal}$ values from the pseudo-second-order and Ritchie kinetic models are very close to each other. The calculated correlation coefficients in the pseudo-second-order kinetic model are for nickel 0.693 and close to

Table 8
Parameters of kinetic model for adsorption of Pb, Cu and Ni on the hybrid

(T = 25°C, C_i = 20 mg L^{-1}, pH = 5, w = 0.06)							
Model	Pseudo-first-order			Pseudo-second-order			$q_{e,\exp}$
Metal	R^2	K_1	$q_{e,\text{cal}}$	R^2	K_2	$q_{e,\text{cal}}$	
Pb	0.921	0.033	6.686	0.999	0.041	16.667	16.583
Cu	0.934	0.031	7.988	0.999	0.027	16.667	16.417
Ni	0.981	0.009	1.808	0.693	0.008	1.757	1.667
Model	Intra-particle diffusion			Ritchie			$q_{e,\exp}$
Metal	R^2	K_{id}	C	R^2	K_R	$q_{e,\text{cal}}$	
Pb	0.706	1.120	4.406	0.926	0.49	16.67	16.583
Cu	0.727	1.116	4.17	0.930	0.33	16.67	16.417
Ni	0.959	0.106	–0.114	0.950	0.01	2.35	1.667

the unit for lead (0.999) and copper (0.999), respectively. In the Ritchie kinetic model, the calculated correlation coefficients for lead, copper and nickel are 0.926, 0.930 and 0.950, respectively.

The obtained rate constant (K_2) of the pseudo-second-order model for metal ions are lower than the rate constant (K_R) of the Ritchie model (Table 8). This shows that the adsorption of metal ions can be represented by the pseudo-second-order model.

According to the calculated correlation coefficients, the obtained K_2 for the adsorption of the Cu(II) ions are lower than Pb(II) ions that indicates the uptake of copper ions onto hybrid from aqueous solution is faster than that of other metals.

5. Conclusion

In this study, the functionalized carbon nanotube-C60 hybrid was tested to absorb heavy metals such as copper, nickel and lead. The experimental data showed that at 30 min, the removal of metals is more than 90%, which can be achieved more than 99% by adjusting the pH for each metal. The best models and correlation coefficients (R^2) are for the lead (D-R, 0.999 and Langmuir, 0.966), copper (D-R, 0.965) and nickel (Freundlich, 0.961 and Temkin, 0.965) because these models are more compatible with experimental data. The best kinetic models are for the lead and copper pseudo-second-order kinetic model and for nickel is a pseudo-first-order kinetic model with correlation coefficients for lead (0.999), copper (0.999) and nickel (0.981). The amount of ΔG at pH 7 for each three metal is negative (reaction spontaneous) and at pH = 5 for lead and copper is negative (reaction spontaneous) and for nickel is positive (reaction non-spontaneous). The amount of ΔH is negative; thus, the reactions are exothermic. The present study shows that the functionalized nanotube-C60 hybrid was successful in removing heavy metals such as copper, nickel and lead from aqueous solutions. It is certain this the hybrid can be used to adsorb heavy metals and other materials, especially in poisoning with heavy metals, both as a medicine and as a drug carrier.

Conflicts of interest

There is no conflict to declare.

Acknowledgments

The authors would like to greatly appreciate Dr. Ahadian and the lab staff, as well as the Institute for Nanoscience & Nanotechnology (INST) of Sharif University of Technology that cooperated for doing this research.

Symbols

C_e — Equilibrium concentration of solution, mg L^{-1}
C_i — Initial concentration of solution, mg L^{-1}
q_e — Amount of metal adsorbed per unit mass of adsorbent at equilibrium, mg g^{-1}
q_m — Langmuir constant, mg g^{-1}
q_t — Amount of metal adsorbed per unit mass of adsorbent at time t, mg g^{-1}
K_F — Freundlich constant, L mg^{-1}
K_L — Langmuir constant, L mg^{-1}
E_a — Dubinin–Radushkevich isotherm constant, kJ mol^{-1}
K_T — Temkin isotherm equilibrium binding constantm, L g^{-1}
K_1 — Rate constant of the pseudo-first-order adsorption process, min^{-1}
K_2 — Rate constant of pseudo-second-order adsorption, g mg^{-1} min^{-1}
K_{id} — Intra-particle diffusion constant, mg g^{-1} min$^{0.5}$
K_{R} — Richie constant, min^{-1}
n — Freundlich constant, L g^{-1}
R — Gas constant, 8.314 J mol^{-1} K^{-1}
T — Temperature, K
β — Mean free energy of adsorption, mol^2 kJ^{-2}
t — Time, min
b_T — Adsorption constant, J mol^{-1} K^{-1}
R — Universal gas constant, 8.314 J mol^{-1}K^{-1}
T — Absolute temperature value, K
B — Constant related to the heat of sorption, J mol^{-1}
w — Weight adsorbent, g

ΔG — Gibbs free energy, kJ mol^{-1}
ΔH — Enthalpy, kJ mol^{-1}
ΔS — Entropy, kJ mol^{-1}

References

[1] M.B. Arian, T.G. Kazi, M.K. Jamali, H.I. Afridi, J.A. Baig, N. Jablini, A.Q. Shah, Evaluation of physico-chemical parameters of Manchar Lake water and their comparison with other global published values, Pak. J. Anal. Environ. Chem., 9 (2008) 101–109.

[2] S. Sanyal, The End of Population Growth, Project Syndicate, 2011 [Online].

[3] UNESCO, Water for a Sustainable World, Retrieved from Paris, 2015.

[4] W.S.W. Ngah, M.A.K.M. Hanafiah, Removal of heavy metal ions from wastewater by chemically modified plant wastes as adsorbents: a review, Bioresour. Technol., 99 (2008) 3935–3948.

[5] S.E. Bailey, T.J. Olin, R.M. Bricka, D.D. Adrian, A review of potentially low-cost sorbents for heavy metals, Water Res., 33 (1999) 2469–2479.

[6] S. Benzer, N. Arslan, N. Uzel, A. Gül, M. Yılmaz, Concentrations of metals in water, sediment and tissues of *Cyprinus carpio* L., 1758 from Mogan Lake (Turkey), Iran. J. Fish. Sci., 12 (2013) 45–55.

[7] F. Moore, G. Orghani, A. Qishla, Assessment of Heavy metal contamination in water and surface sediments of the Maharlu saline Lake, SW Iran, Iran. J. Sci. Technol. Trans. A Sci., 33 (2009) 44–54.

[8] G. Sharma, B. Thakur, Mu. Naushad, A.H. Al-Muhtaseb, A. Kumar, M. Sillanpaa, G.T. Mola, Fabrication and characterization of sodium dodecyl sulphate@ironsilicophosphate nanocomposite: ion exchange properties and selectivity for binary metal ions, Mater. Chem. Phys., 193 (2017) 129–139.

[9] D. Pathania, G. Sharma, Mu. Naushad, A. Kumar, Synthesis and characterization of a new nanocomposite cation exchanger polyacrylamide Ce(IV) silicophosphate: photocatalytic and antimicrobial applications, J. Ind. Eng. Chem., 20 (2014) 3596–3603.

[10] Mu. Naushad, S. Vasudevan, G. Sharma, A. Kumar, Z.A. ALOthman, Adsorption kinetics, isotherms, and thermodynamic studies for Hg^{2+} adsorption from aqueous medium using alizarin red-S-loaded amberlite IRA-400 resin, Desal. Wat. Treat., 57 (2016) 18551–18559.

[11] Md.R. Awual, Md.M. Hasan, G.E. Eldesoky, Md.A. Khaleque, M.M. Rahman, Mu. Naushad, Facile mercury detection and removal from aqueous media involving ligand impregnated conjugate nanomaterials, Chem. Eng. J., 290 (2016) 243–251.

[12] G. Annadurai, R.S. Juang, D.J. Lee, Adsorption of heavy metals from water using banana and orange peels, Water Sci. Technol., 47 (2003) 185–190.

[13] G.P. Rao, C. Lu, F. Su, Sorption of divalent metal ions from aqueous solution by carbon nanotubes: a review, Sep. Purif. Technol., 58 (2007) 224–231.

[14] S. Sabat, R.V. Kavitha, S.L. Shantha, G. Nair, M. Ganesh, N. Chandroth, Biosorption: an eco-friendly technique for the removal of heavy metals, Ind. J. Appl. Res., 2 (2012) 1–8.

[15] Z.A. Al-Othman, R. Ali, Mu. Naushad, Hexavalent chromium removal from aqueous medium by activated carbon prepared from peanut shell: adsorption kinetics, equilibrium and thermodynamic studies, Chem. Eng. J., 184 (2012) 238–247.

[16] V.K.K. Upadhyayula, S.G. Deng, M.C. Mitchell, G.B. Smith, Application of carbon nanotube technology for removal of contaminants in drinking water: a review, Sci. Total Environ., 408 (2009) 1–13.

[17] J.-G. Yu, X.-H. Zhao, L.-Y. Yu, F.-P. Jiao, J.-H. Jiang, X.-Q. Chen, Removal, recovery and enrichment of metals from aqueous solutions using carbon nanotubes, J. Radioanal. Nucl. Chem., 299 (2014) 1155–1163.

[18] N. Mubarak, J. Sahu, E. Abdullah, N. Jayakumar, Removal of heavy metals from wastewater using carbon nanotubes, Sep. Purif. Rev., 43 (2014) 311–338.

[19] X. Ren, C. Chen, M. Nagatsu, X. Wang, Carbon nanotubes as adsorbents in environmental pollution management: a review, Chem. Eng. J., 170 (2011) 395–410.

[20] M.E. Milanesio, M.B. Spesia, M.P. Cormick, E.N. Durantini, Mechanistic studies on the photodynamic effect induced by a dicationic fullerene C60 derivative on Escherichia coli and Candida albicans cells, Photodiagn. Photodyn. Ther., 10 (2013) 320–327.

[21] X. Tao, Y. Yu, J.D. Fortner, Y. He, Y. Chen, J.B. Hughes, Effects of aqueous stable fullerene nanocrystal (nC60) on Scenedesmus obliquus, Chemosphere, 122 (2014) 162–167.

[22] Q. Liu, Q. Cui, X.J. Li, L. Jin, The applications of buckminsterfullerene C60 and derivatives in orthopaedic research, Connect. Tissue Res., 55 (2014) 71–79.

[23] A. Hirsch, C. Bellavia-Lund, C60s and Related Structures, A. Hirsch Eds., Springer Publications, Berlin, 1993.

[24] Q.-H. Weng, Q. He, T. Liu, H.-Y. Huang, J.-H. Chen, Z.-Y. Gao, L.-S. Zheng, Simple combustion production and characterization of octahydro[60]fullerene with a non-IPR C60 cage, J. Am. Chem. Soc., 132 (2010) 15093–15095.

[25] Y. Chai, T. Guo, C. Jin, R.E. Haufler, L.F. Chibante, J. Fure, R.E. Smalley, C60s with metals inside, J. Phys. Chem., 95 (1991) 7564–7568.

[26] H. Paloniemi, T. Aaritalo, T. Laiho, H. Liuke, N. Kocharova, K. Haapakka, F. Terzi, R. Seeber, J. Lukkari, Water-soluble full-length single-wall carbon nanotube polyelectrolytes: preparation and characterization, J. Phys. Chem. B, 109 (2005) 8634–8642.

[27] L D. E. Luzzi, B. W. Smith, and M. Monthioux., Encapsulated C60 in carbon nanotubes, Nature , 396(1998) 323–324.

[28] A.B. Bourlinos, V. Georgakilas, A. Bakandritsos, A. Kouloumpis, D. Gournis, R. Zbori, Aqueous-dispersible fullerol-carbon nanotube hybrids, Mater. Lett., 82 (2012) 48–50.

[29] en.wikipedia.org/wiki/Solubility_table, 2018.

[30] D.D. Amarendra, P.D. Shashi, G. Krishna, S. Mika, Strengthening adsorptive amelioration: isotherm modeling in liquid phase surface complexation of Pb (II) and Cd (II) ions, Desalination, 267 (2010) 25–33.

[31] A.B. Albadarin, M.N. Collins, Mu. Naushad, S. Shirazian, G. Walker, C. Mangwandi, Activated lignin-chitosan extruded blends for efficient adsorption of methylene blue, Chem. Eng. J., 307 (2017) 264–272.

[32] A. Farah, P. John, A. Iqbal, Microbes and Microbial Technology: Agricultural and Environmental Applications, Springer Publications, New York, 2011.

[33] Y.S. Ho, G. McKay, Competitive sorption of copper and nickel ions from aqueous solution using peat, Adsorption, 5 (1999a) 409–417.

[34] R. Prabakaran, S. Arivoli, Biosorption of ferrous ion from aqueous solutions by using activated carbon prepared from Thespesia populnea bark, Arch. Appl. Sci. Res., 3 (2011) 218–232.

[35] K.G. Bhattacharyya, A. Sharma, Adsorption of Pb(II) from aqueous solution by Azadirachta indica (neem) leaf powder, J. Hazard. Mater., B,113 (2004) 97–109.

[36] T.M. Elmorsi, Equilibrium isotherms and kinetic studies of removal of methylene blue dye by adsorption onto miswak leaves as a natural adsorbent, J. Environ. Prot., 2 (2011) 817–827.

[37] H.M.F. Freundlich, Over the adsorption in solution, Phys. Chem., 57 (1906) 385–471.

[38] M.M. Dubinin, L.V. Radushkevich, The equation of the characteristic curve of activated charcoal, Proceedings of the Academy of Sciences, Phys. Chem. Sec., 55 (1947) 331–337.

[39] W. Rondon, D. Freire, Z. de Benzo, A.B. Sifontes, Y. González, M. Valero, J.L. Brito, Application of 3A zeolite prepared from venezuelan kaolin for removal of Pb (II) from wastewater and its determination by flame atomic absorption spectrometry, Am. J. Anal. Chem., 4 (2013) 584–593.

[40] H. Chen, J. Zhao, G. Dai, J. Wu, H. Yan, Adsorption characteristics of Pb(II) from aqueous solution onto a natural biosorbent,

fallen Cinnamomum camphora leaves, Desalination, 262 (2010) 174–182.
[41] A.N. Siyal, S.Q. Memon, M.I. Khaskheli, Optimization and equilibrium studies of Pb(II) removal by Grewia Asiatica seed: a factorial design approach, Pol. J. Chem. Technol., 14 (2012) 71–77.
[42] S.N. Dash, R. Murthy, Preparation of carbonaceous heavy metal adsorbent from Shorea robusta leaf litter using phosphoric acid impregnation, Environ. Sci., 1 (2010) 296–313.
[43] M. Ghasemi, Mu. Naushad, N. Ghasemi, Y. Khosravi-Fard, Adsorption of Pb(II) from aqueous solution using new adsorbents prepared from agricultural waste: adsorption isotherm and kinetic studies, J. Ind. Eng. Chem., 20 (2014) 2193–2199.
[44] Mu. Naushad, Surfactant assisted nano-composite cation exchanger: development, characterization and applications for the removal of toxic Pb^{2+} from aqueous medium, J. Chem. Eng., 235 (2014) 100–108.
[45] Mu. Naushad, Z.A. ALOthman, Md.R. Awual, M.M. Alam, G.E. Eldesoky, Adsorption kinetics, isotherms, and thermodynamic studies for the adsorption of Pb^{2+} and Hg^{2+} metal ions from aqueous medium using Ti(IV) iodovanadate cation exchanger, Ionics, 21 (2015) 2237–2245.
[46] M. Ghasemi, Mu. Naushad, N. Ghasemi, Y. Khosravi-Fard, A novel agricultural waste based adsorbent for the removal of Pb(II) from aqueous solution: kinetics, equilibrium and thermodynamic studies, Ind. Eng. Chem., 20 (2014) 454–461.
[47] A. Mittal, Mu. Naushad, G. Sharma, Z.A. ALothman, S.M. Wabaidur, M. Alam, Fabrication of MWCNTs/ThO_2 nanocomposite and its adsorption behavior for the removal of Pb(II) metal from aqueous medium, Desal. Wat. Treat., 57 (2016) 21863–21869.
[48] R. Bushra, Mu. Naushad, R. Adnan, M.N.M. Brahim, M. Rafatullah, Polyaniline supported nanocomposite cation exchanger: synthesis, characterization and applications for the efficient removal of Pb^{2+} ion from aqueous medium, Ind. Eng. Chem., 21 (2015) 1112–1118.
[49] Y. Gutha, V.S. Munagapati, Mu. Naushad, K. Abbur, Removal of Ni(II) from aqueous solution by Lycopersicum esculentum (tomato) leaf powder as a low-cost biosorbent, Desal. Wat. Treat., 54 (2015) 200–208.
[50] M.A. Shavandi, Z. Haddadian, M.H. Ismail, S.N. Abdullah, Z.Z. Abidin, Continuous metal and oil removal from palm oil mill effluent using natural zeolite-packed column, J. Taiwan Inst. Chem. Eng., 43 (2012) 934–941.
[51] Y.S. Ho, G. McKay, The sorption of lead(II) ions on peat, Water Res., 33 (1999) 578–584.
[52] T.W. Weber, R.K. Chatravorti, Pore and solid diffusion models for fixed-bed adsorbers, J. Am. Inst. Chem. Eng., 20 (1974) 228–238.
[53] AG. Ritchie, Alternative to the Elovich equation for the kinetics of adsorption of gases on solids, Faraday Trans., 73 (1977) 1650–1653.